

Geophysical Research Letters

RESEARCH LETTER

10.1029/2019GL082780

Key Points:

- Aftershocks of M≥3 following the 2016 M7.8 Kaikōura earthquake are relocated using data from temporary and permanent seismic networks
- Aftershocks almost exclusively cluster in the shallow crust and are laterally more continuous than mapped surface ruptures
- Shallow (<10-km depth) aftershocks highlight linkages at depth between surface-rupturing fault segments

Supporting Information:

- Supporting Information S1
- · Table S1
- · Movie S1
- Data Set S1

Correspondence to:

F. Lanza, flanza@wisc.edu

Citation:

Lanza, F., Chamberlain, C. J., Jacobs, K., Warren-Smith, E., Godfrey, H. J., Kortink, M., et al. (2019). Crustal fault connectivity of the $\rm M_w$ 7.8 2016 Kaikōura earthquake constrained by aftershock relocations. *Geophysical Research Letters*, 46. https://doi.org/10.1029/2019GL082780

Received 11 MAR 2019 Accepted 17 MAY 2019 Accepted article online 28 MAY 2019

Crustal Fault Connectivity of the $M_{\rm w}$ 7.8 2016 Kaikōura Earthquake Constrained by Aftershock Relocations

F. Lanza¹, C. J. Chamberlain², K. Jacobs³, E. Warren-Smith³, H. J. Godfrey^{2,3}, M. Kortink², C. H. Thurber¹, M. K. Savage², J. Townend², S. Roecker⁴, and D. Eberhart-Phillips⁵

¹Department of Geoscience, University of Wisconsin-Madison, Madison, WI, USA, ²School of Geography, Environment, and Earth Sciences, Victoria University of Wellington, Wellington, New Zealand, ³GNS Science, Lower Hutt, New Zealand, ⁴Earth and Environmental Sciences, Rensselaer Polytechnic Institute, Troy, NY, USA, ⁵GNS Science, Dunedin, New Zealand

Abstract The 14 November $2016 \, M_w 7.8 \, Kaik \bar{o}$ ura earthquake in the northern South Island, New Zealand, involved highly complex, multifault rupture. We combine data from a temporary network and the permanent national seismograph network to repick and relocate ~2,700 aftershocks of M≥3 that occurred between 14 November 2016 and 13 May 2017. Automatic phase-picking is carried out using REST, a newly developed hybrid method whose pick quality is assessed by comparing automatic picks for a subset of 138 events with analysts' picks. Aftershock hypocenters computed from high-quality REST picks and a 3-D velocity model cluster almost exclusively in the shallow crust of the upper plate and reveal linkages at depth between surface-rupturing fault segments. Only eight aftershocks are relocated on a deeper structure positioned between patches of geodetically detected afterslip. This indicates that afterslip has not triggered significant earthquake activity on the subduction interface during the period of aftershock activity analyzed.

Plain Language Summary Earthquake locations are fundamental for understanding the physics of earthquakes, defining the orientations and geometries of faults that have slipped seismically, and assisting in seismic hazard forecasting and assessment. We have mapped the locations of approximately 2,700 of the largest aftershocks that followed the 14 November 2016 M_w 7.8 Kaikōura earthquake in the northern South Island, New Zealand. We achieve improvements in the precision and accuracy of the earthquakes' relocated hypocenters in two ways: (1) by using an expanded seismic network that incorporates data from more stations and (2) by applying a new automatic picking methodology that produces better seismic wave arrival time estimates. Our results show that most of the seismic energy released in the 6 months following the mainshock was generated in the uppermost 20 km of the crust, with the aftershocks' locations suggesting that separate faults mapped at the surface are in fact continuous at greater depth. Very little earthquake energy is associated with the subduction interface.

1. Introduction

In the past decade, the central and northern regions of New Zealand's South Island have been struck by several damaging earthquakes, including the Mw7.1 Darfield and Mw6.2 Christchurch earthquakes of 2010 and 2011 (Bannister & Gledhill, 2012; Gledhill et al., 2011); the Mw6.6 Seddon and Mw6.7 Lake Grassmere earthquakes of 2013 (Hamling et al., 2014; Holden et al., 2013); and, most recently, the M_w7.8 Kaikōura earthquake of 14 November 2016. The Kaikōura earthquake stands out as one of the most complex earthquakes recognized worldwide (Hamling et al., 2017), with surface rupture mapped on at least 20 faults (Litchfield et al., 2018). The ruptured region straddles a complex tectonic transition from subduction of the Pacific Plate beneath the Australian Plate to strike-slip and continental collision along the Alpine Fault in the central South Island (Figure 1a). The earthquake nucleated near The Humps Fault at a depth of 14 km (Nicol et al., 2018), ~20 km south of the Hope Fault, in the transpressional North Canterbury Domain, and propagated ~180 km northeastward in the predominantly strike-slip Marlborough Fault System, before arresting offshore near Cape Campbell (Clark et al., 2017; Hamling et al., 2017; Hollingsworth et al., 2017; Kearse et al., 2018; Litchfield et al., 2018; Nicol et al., 2018; Wang et al., 2017; Williams et al., 2018; Figures 1b and 1c). Surface fault displacement peaked at ~12 m of dextral slip on the Kekerengu Fault (Litchfield et al., 2018). The mainshock also induced widespread coastal uplift and an associated small tsunami (Clark et al., 2017; Gusman et al., 2018; Hamling et al., 2017; Power et al., 2017).

©2019. American Geophysical Union. All Rights Reserved.

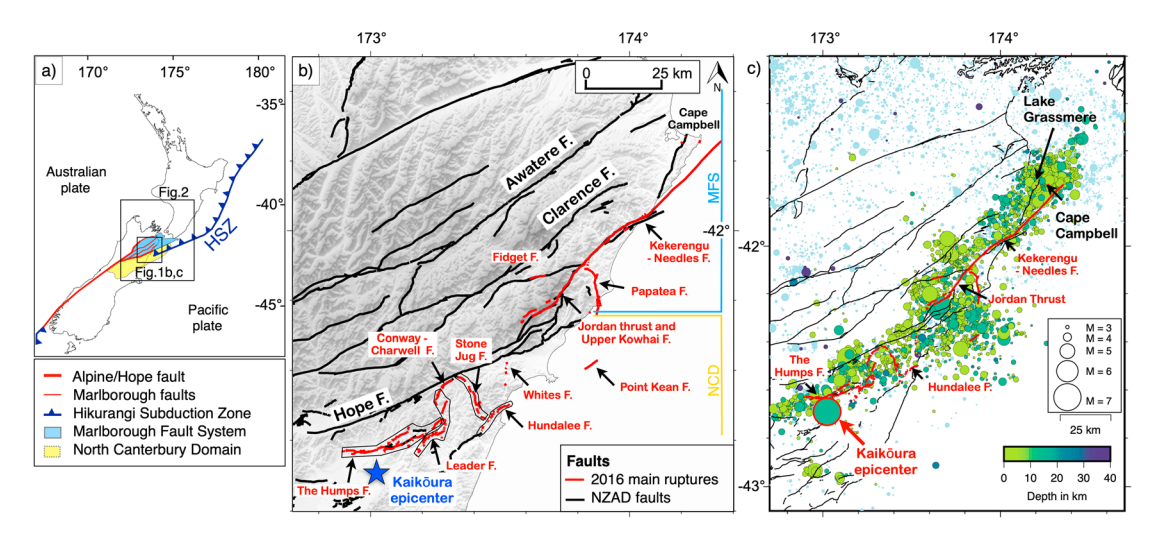


Figure 1. (a) Map showing the plate boundary setting of the Kaikōura earthquake. (b) Map of the faults that ruptured during the 2016 M_w 7.8 Kaikōura earthquake (red lines, from Hamling et al., 2017) along with the previously identified active faults (black lines, from Langridge et al., 2016). The blue star indicates the earthquake epicenter location from the GeoNet catalog. (c) Map of the ~2700 earthquake epicenters selected from the GeoNet catalog, including the mainshock, to use in the relocation analysis. The light-blue circles indicate relocated background seismicity from Eberhart-Phillips et al. (2014) from 2001 to 2011.

In addition to complex shallow rupture on upper plate faults, some studies have suggested that the underlying subduction interface contributed to the mainshock moment release. Some authors argue that the subduction interface contributed >50% of the earthquake's moment (Bai et al., 2017; Duputel & Rivera, 2017; Hollingsworth et al., 2017; Wang et al., 2017), whereas others argue for a smaller contribution (<30%; Clark et al., 2017; Hamling et al., 2017), or no contribution at all (Cesca et al., 2017; Gusman et al., 2018; Xu et al., 2018).

Beneath the coastal Marlborough region, the subducted Pacific slab underlies Mesozoic accretionary terranes (Eberhart-Phillips et al., 2014; Wallace et al., 2018; Wannamaker et al., 2009). Geodetic inversions reveal smooth patterns of velocities that can be fit by a simple model of elastic distortion due to deep slip on a single plate interface extending from the North Island to the Kaikōura region, with a locking depth that varies smoothly across the region (Lamb et al., 2018; Lamb & Smith, 2013). Thus, strain is thought to be focused in the ductile lower crust above the Pacific slab, loading the Marlborough faults (Eberhart-Phillips et al., 2014; Wallace et al., 2018; Wannamaker et al., 2009). The slab seismicity is laterally near-continuous throughout this same region, suggesting a similarly continuous subducted plate (Evanzia et al., 2018; Reyners et al., 2011; Williams et al., 2013). Following the Kaikōura earthquake, long-wavelength features in the postseismic GPS and InSAR observations were interpreted by Wallace et al. (2018) to suggest that ~0.5 m of afterslip had occurred between November 2016 and December 2017 on the subduction interface.

Aftershock activity located by New Zealand's geological hazard monitoring center, GeoNet (Figure 1c), highlights structures that ruptured coseismically, including The Humps and Hundalee faults, in a broad NE-SW trend. The activity steps northwest to follow the Papatea Fault's strike and then continues along the Kekerengu Fault. North of the Kekerengu Fault, where rupture is also observed offshore (Kearse et al., 2018), the GeoNet catalog reveals a cluster of events near Cape Campbell and Lake Grassmere (Figure 1c). The existing GeoNet catalog locations (as of 6 November 2018, when last accessed) are of insufficient quality to define many of the smaller fault structures. Likewise, the location accuracy does not elucidate whether the shallow faults are connected at depth or whether there is seismic activity on the subduction interface. This limitation of the GeoNet catalog arises primarily from the sparse station coverage, inaccurate automatic phase-picks, and the simplified velocity models used for some routine locations.

To identify smaller, shallow fault structures, address whether they are connected at depth, and study relationships between aftershocks and afterslip on the subduction interface, we present a new set of high-precision aftershock relocations. Relocations are carried out using a recently developed method for automated detection and onset estimation (REST: Thurber et al., 2017; see Text S1) and updated 3D Vp and Vp/Vs New Zealand-wide (v2.1) velocity models (Eberhart-Phillips et al., 2017; Eberhart-Phillips &



Reyners, 2012). These results constitute the first step toward elucidating the geometry and interconnectedness of fault structures active during the aftershock sequence.

2. Data Sets

We repick and relocate \sim 2,700 events with local magnitudes of $M_L \ge 3$ that occurred between 13 November 2016 and 13 May 2017 (UTC) in a rectangular region between latitudes -43.00 and -40.80° and longitudes 172.75 and 175.20°. These earthquakes were previously analyzed and manually reviewed by GeoNet, who computed origin times, locations, magnitudes, and depths (Figure 1c).

We use data from both a temporary aftershock network, Seismic Triggering Response for Earthquakes around Wellington NZ (STREWN), deployed in northern South Island and southern North Island (Figure S1 in the supporting information), and selected GeoNet permanent instruments (Petersen et al., 2011; Table S1). The 24 STREWN instruments were operational for ~6 months from late November 2016 until early May 2017. Of the available GeoNet stations, we used a combination of short-period, broadband, and strong motion data for sites within ~300 km of Cape Campbell.

3. Methods

Accurate identification of phase arrival times is essential to assuring high-precision earthquake locations in standard workflows. We introduce here (see Text S1) a hybrid method for automated detection and onset estimation, called REST, which combines a modified version of the nearest-neighbor similarity scheme of Rawles and Thurber (2015) with the autoregressive approach of Kushnir et al. (1990). We obtain accuracy information on the REST algorithm by comparing autopicks with picks made by analysts for a subset of earthquakes and to picks obtained with the nonparametric autopicker method of Rawles and Thurber (2015), *kpick* (Text S1).

After excluding all the S picks with arrival time uncertainties >0.6 s, as well as all the unpaired S wave arrivals, a total of 114,140 automatic P and 73,783 automatic S picks remained for the relocation analysis.

We performed initial aftershock relocations using the seismic tomography code simul2014, extended from simulps12/simul2000 (Eberhart-Phillips & Reyners, 2012; Eberhart-Phillips & Bannister, 2015; Evans et al., 1994; Thurber & Eberhart-Phillips, 1999). Simul2014 uses a 3-D velocity model and a linearized earthquake location method; when relocating we did not allow the velocity model to vary. We also attempted to locate the seismicity using the probabilistic nonlinear global-search inversion approach of Lomax et al. (2009), NonLinLoc, but obtained poorer fits to the data in the Kaikōura and epicentral regions where station coverage is sparser and the velocity model is less well constrained (see Text S2). The locations obtained from simul2014 were used as initial input for hypoDD 3D (v2.1b), which uses the double-difference algorithm of Waldhauser and Ellsworth (2000) with a 3-D velocity model and cross-correlation differential times to produce final high-precision hypocenter locations.

4. Relocation Results

4.1. Initial Earthquake Location

For the linearized earthquake relocation inversion using simul2014, we employ the same New Zealand-wide inversion grid used in v2.1 of the 3-D velocity model (Eberhart-Phillips et al., 2017; Eberhart-Phillips & Reyners, 2012), but for a smaller region (340 km \times 500 km) centered on our study area. The 3-D Vp and Vp/Vs models were used as fixed velocity models. A standard weighting scheme from 0 to 4 was employed in which the highest weight was assigned to picks with uncertainties of <0.02 s (i.e., the highest-quality picks) and the lowest weight was given for pick uncertainties of >0.5 s.

Figure 2 shows the earthquake relocations (filled yellow circles). The weighted root-mean-square misfit is reduced from 0.31 to 0.23 s, a reduction of ~26% with respect to the initial locations obtained from the REST algorithm during the picking phase. A total of 110 events have poor depth constraints and were not considered further. The remaining 2,655 events are located close to mapped surface faults (Figure 2). The relocated hypocentral depths are distinctly shallower than the modeled subduction interface of Williams et al. (2013), which was derived from the locations of a 10-year relocated earthquake catalog (Reyners

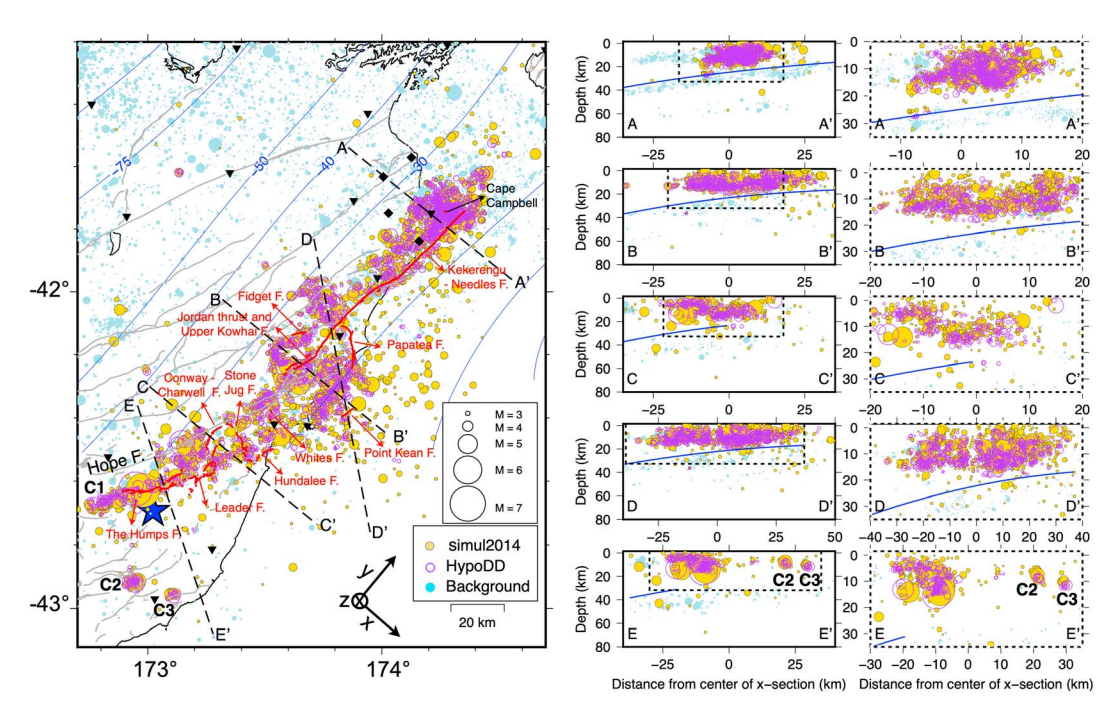


Figure 2. Map view and cross sections of the earthquake relocations using simul2014 (2655 yellow circles) and hypoDD (2013 clustered open purple circles). Relocated background seismicity from 2001 to 2011 (light-blue circles) is from Eberhart-Phillips et al. (2014). For the cross-sections, each panel shows projected earthquakes within 20 km of the cross-section line, and the rightmost panels are zooms within the cross sections along the same profile as indicated by the dashed box in the center panels. The blue star indicates the Kaikōura epicenter from the Geonet catalog, and the blue solid lines indicate the subduction interface contours from Williams et al. (2013). Arrows in the lower right corner shows the model-aligned x, y, and z directions.

et al., 2011). The aftershocks tend to cluster in the top 20 km of the crust, mimicking the background relocated seismicity of Eberhart-Phillips et al. (2014) at those depths (Figure 2).

4.2. Double-Difference Earthquake Relocation

The dynamically weighted double-difference inversion of the simul2014-relocated data set uses 1,359,256 phase-derived differential times and 187,138 cross-correlation-derived differential times calculated between pairs of events with a maximum hypocenter separation of 10 km and a normalized cross-correlation coefficient >0.65. We compute cross correlations in the time domain using filtered (1–20 Hz) seismogram pairs of 1-s duration spanning each P and S arrivals and beginning 0.2 s before the pick time. The maximum hypocenter separation allowed of 10 km discards 24% of the events, reducing the number of relocated events from 2,655 to 2013 (open purple circles in Figure 2). Because the uncertainties in the final locations estimated by hypoDD using the LSQR method are grossly underestimated (Waldhauser & Ellsworth, 2000), we assess them independently using a bootstrap resampling method (Mesimeri et al., 2018) in which relocation is repeated for 100 samples. The median 95% confidence error ellipse semimajor axis lengths for all the events are \sim 592, 358, and 426 m in the model-aligned x, y, and z directions, respectively. HypoDD relocations also cluster in the top 20 km of the crust and form tighter clusters (Figures 2 and S9) than the simul2014 results. Many of the discarded nonclustered events lie offshore from the central rupture area and cannot be located with high accuracy. Thus, we cannot evaluate potential offshore fault structures.

5. Discussion

5.1. Relationship Between Aftershock Locations and Surface Ruptures

The relocated aftershock sequence shows a general spatial agreement with the relocated background crustal seismicity (Eberhart-Phillips et al., 2014), for which a similar 3-D velocity model and location method were used (Figure 2). The relocated epicenter of the mainshock has latitude of –42.62° and longitude of 172.95°: it is located within the aftershocks associated with The Humps Fault at a depth of ~15 km, which together delineate a more vertical plane than the projection of the fault (Figures 2 and 3a and Movie S1 in the supporting information) based on Litchfield et al.'s (2018) results. This is in contrast with the relocated mainshock

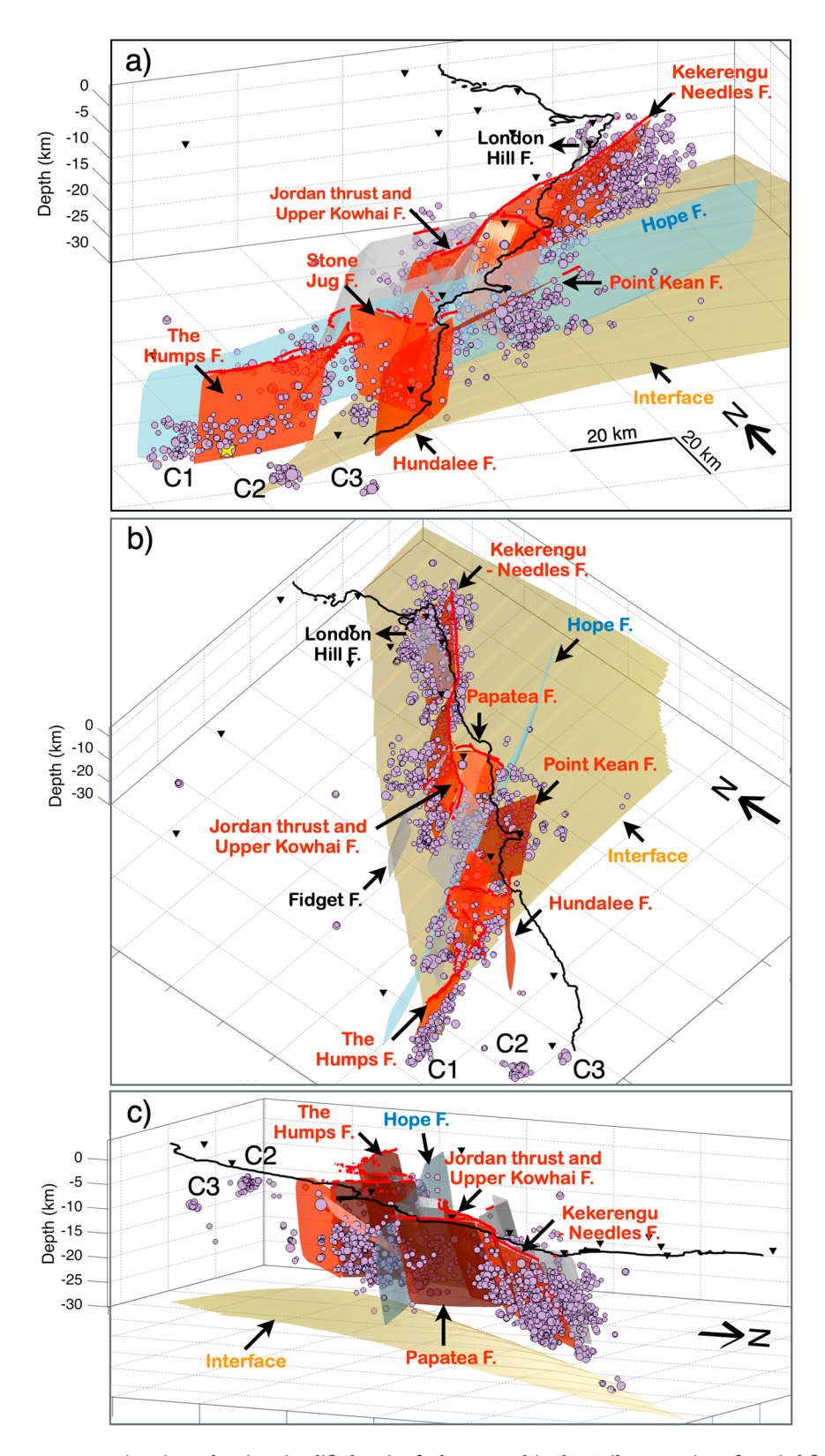


Figure 3. 3-D perspective views showing simplified major faults mapped in the Kaikōura region after Litchfield et al. (2018), the subduction interface after Williams et al. (2013), and our aftershock relocations. (a) Oblique map view, towards north; (b) oblique view towards northeast; c) oblique view towards south. Red indicates faults that ruptured during the mainshock, whereas gray indicates other mapped active faults. A video showing the 3-D rotation of this figure is provided in the SM.



hypocenter obtained by Nicol et al. (2018), which lies at a similar depth to our relocated hypocenter but south of the fault projection, and which Nicol et al. (2018) used to argue for a 80°S dip of The Humps Fault in its western section. Our relocations in this area are compatible with the average strike of first motion solution in this region found by Cesca et al. (2017) but lie on a more steeply dipping plane in our model.

Events relocated near Cape Campbell, where the station coverage is good, are well constrained, with agreement between the results obtained using all the location algorithms, including NonLinLoc (Text S2 and Figures S6-S8). Most of the events near Cape Campbell are clearly located above the inferred subduction interface, except for eight events (see section 5.2) that cluster on the eastern/updip side of the main afterslip patch identified by Wallace et al. (2018; Figures 2A-A' and 4). Although most of the events near Cape Campbell lie close to the London Hill and Kekerengu-Needles fault plane projections presented by Litchfield et al. (2018), some extend over a wider area, possibly including subsidiary offshore structures in the Cook Strait (Figures 3a and 3c). A similar pattern was also observed for the 1990-2001 local background seismicity (Du et al., 2004) and the 2013 Seddon and Lake Grassmere earthquakes (Hamling et al., 2014; Holden et al., 2013). We note that Cesca et al. (2017) resolved an average strike of 248° (similar to that found by Kaiser et al., 2017) in this region from moment tensor analysis, which is ~23° clockwise of the strike of the Needles Fault (Kearse et al., 2018). We hypothesize that this strike could reflect the strike of linking structures at depth between the London Hill and Needles faults as reflected by the diffuse aftershock pattern found here. In general, the majority of the relocated aftershocks lies close to mapped surface ruptures and their inferred depth projections (Litchfield et al., 2018), with the exception of the Point Kean Fault, which might be more steeply dipping (Figure 3a). This is in contrast with Mouslopoulou et al.'s (2019) relocation study, where the Point Kean Fault and a newly identified fault, referred to by those authors as the Offshore Splay Thrust Fault, delineate shallower offshore structures that are not revealed by our analysis. Our final relocated catalog comprises all but seven events used in Mouslopoulou et al. (2019) in the region of the Offshore Splay Thrust Fault, thus, although higher location uncertainties characterize this central rupture area (Figure S10), our study does not provide evidence for the presence of extensive offshore faulting structures.

Onshore, the aftershock relocations reveal some regions in which seismicity is more continuous than mapped surface ruptures: Figures 2 and 3a show that aftershocks are distributed continuously south of the southwest tip of The Humps Fault (cluster C1; Figure 2), possibly indicating an extension of the fault to the southwest. Similar continuity is also detected between The Humps and the Conway-Charwell faults (Figure 2). A fault-perpendicular cluster located at depths of 8–16 km connects the Upper Kowhai Fault to the Fidget Fault (Figure 3b). The connectivity of structures at depth suggests that coseismic slip may have occurred in these regions without a recognized surface expression. The more continuous seismicity patterns may also indicate the presence of active faults, small connecting segments, or more randomly oriented and unconnected fractures that did not rupture to the surface during the mainshock but which may have had a role in transferring stress to the northeast fault structures. Interestingly, the Hope Fault, which had limited surface rupture during the mainshock (Clark et al., 2017) and which is modeled to have experienced a negative change in Coulomb failure stress (Hamling et al., 2017), is active early in the sequence, between November 2016 and January 2017 (Figure S13). Hamling et al. (2017) and Clark et al. (2017) inferred limited coseismic slip to have occurred on the Hope Fault. However, the presence of early aftershocks may indicate that the mainshock did indeed trigger subsurface slip on the Hope Fault.

Also noteworthy is that the oblique, reverse-sinistral Papatea Fault, which produced ~5–6 m of strike-slip and 6–7 m of dip-slip displacement coseismically (Hamling et al., 2017), is quiet during the aftershock sequence (Figures 3b and 3c). This absence of aftershocks was observed by Hamling et al. (2017), who interpreted the coseismic offset as a pop-up structure within a restraining bend between the Jordan Thrust and the Kekerengu Fault. Hamling et al. (2017) also observed negligible postseismic vertical deformation across the fault, which, coupled with the lack of aftershocks, suggest no postseismic motion has occurred on this fault.

Lastly, two clusters of seismicity southeast of the epicenter (C2 and C3 in Figures 2 and 3a–3c) are distinctive because of their locations and because, unlike most of the aftershocks, they are spatially distinct from the locations of background seismicity. The clusters are near several active fault structures (Mount Culverden, Mount Alexander, Scargill Creek, Greta Valley, and Blythe faults) not known to have ruptured during the

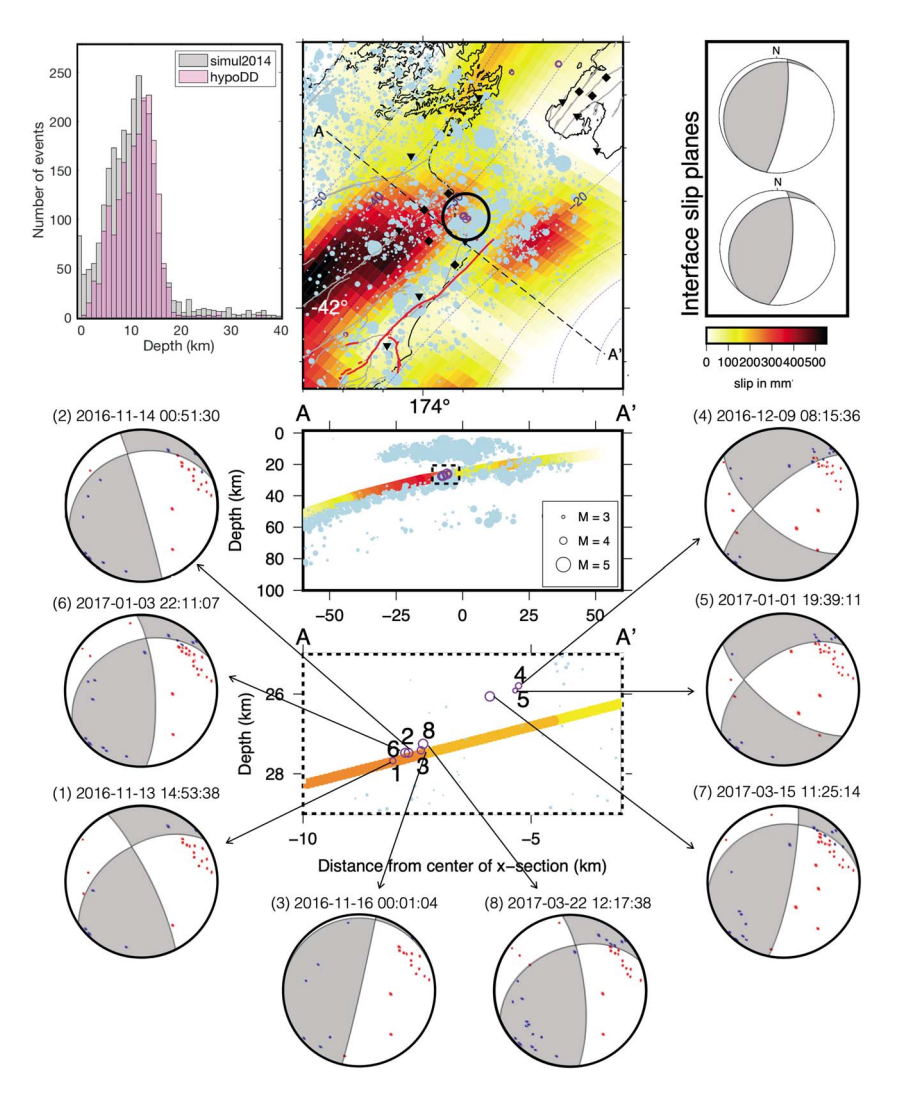


Figure 4. Focal mechanisms for eight events located close to the subduction interface. Stereonets are lower hemispheric projections. We show solutions for the depths obtained by the hypoDD relocation method only. The beachballs in the top right panel are mechanisms expected from using strike, dip, and rake values for post-Kaikōura interface slip of Wallace et al. (2018). The color scale for afterslip on the plate interface for mid-November 2016 to mid-January 2017 is from Wallace et al. (2018). Relocated background seismicity from 2001 to 2011 (light blue circles) is from Eberhart-Phillips et al. (2014).

mainshock. Cluster C3 is active later in the aftershock sequence (February–March 2017), and it could be related to stresses induced by the ruptures of the northern structures. Conversely, C2 is entirely composed of events that occurred in November 2016, within 2 weeks of the mainshock (Figure S13), indicating a possible relation with the mainshock itself.

5.2. Role of the Subduction Interface

One of the outstanding questions surrounding the Kaikōura earthquake concerns the interaction of upper plate faults with the underlying subducted plate. Time-dependent inversions of GPS and InSAR data suggest widespread triggering of slow-slip events on the Hikurangi subduction interface beneath the North Island and large (~0.5 m) afterslip on the subduction interface directly beneath the rupture area (Jiang et al., 2018; Wallace et al., 2018). Wallace et al. (2018) showed that the large-scale postearthquake deformation in the South Island can be explained by displacement on the subduction interface, with the primary patch at 40-km depth down-dip from the Kaikōura earthquake region, and a smaller patch extending to 25-km depth directly under the southern part of the rupture.



Our relocations cluster almost exclusively in the mid-to-upper crust with 92% of the simul2014 locations and 99% of hypoDD locations occurring above 18 km (Figure 4), indicating that the mapped afterslip from Wallace et al. (2018) is mainly occurring aseismically. Only eight events (M_I 3.1–4.1) in our hypoDD event catalog appear to be located near the subduction interface (Figure 4). Using the same 3-D model adopted for the relocations, we calculate focal mechanisms for these events to clarify their relationship with the subduction interface. Automatically picked polarities were reviewed manually and used as input to the Bayesian focal mechanism inversion of Walsh et al. (2009). All mechanisms except the two shallowest ones have one well-constrained shallowly west dipping plane, consistent with the local dip of the subduction interface (Williams et al., 2013), and display predominantly reverse motion with subordinate strike-slip (Figure 4). Conversely, events 4 and 5 show a more dominantly strike-slip mechanism. The resolved slip planes (average strike of 252° and dip of 31°, excluding events 4 and 5; Table S2) are compatible with that of the modeled subduction interface slip planes used by Wallace et al. (2018) in the afterslip modeling: they used two planes with a common strike of 221° and dips of 12° (above 26-km depth) and 23° (below 26-km depth). However, the strikes of the shallow dipping planes of the obtained focal mechanisms are rotated ~20–30° anticlockwise from the local strike of the interface mapped by Williams et al. (2013; Figure 4). Given uncertainties in the interface geometry, we consider it likely that these events occurred on the interface.

We note that the eight putative interface events occur between two patches of high-rate afterslip modeled by Wallace et al. (2018; Figure 4) and lie within a zone of background seismicity. This could suggest the presence of persistent seismic asperities surrounded by aseismically creeping patches. The Kaikōura earthquake sequence may have transferred stress to the upper plate, and leaves open the possibility of the subduction interface being seismically active in the future.

6. Conclusions

Relocation of the Kaikōura aftershock sequence using temporary and permanent seismic network data and improved phase-picking has improved the definition of the active fault geometries. The relocations show that the aftershocks mirror the complexity of surface faulting, with seismicity clustering near inferred fault projections in the midcrust. They also show seismic connections at depth between spatially distinct mapped surface ruptures. In particular, the presence of aftershocks near fault segments associated with the Hope Fault early in the sequence indicates that despite the lack of surface rupture, slip on the fault occurred at depth between the Conway-Charwell and Papatea faults, at least postseismically, and possibly played a role in transferring stress to the northeast fault structures. There is little seismic evidence in our catalog to suggest early postseismic rupture on the subduction interface or any shallowly dipping structure, with 99% of the earthquakes occurring above 18-km depth, and <0.5% of events inferred to be located on the interface. However, the locations and focal mechanism analysis of eight events that do occur near the subduction interface beneath Cape Campbell support the suggestion that this portion of the plate interface is capable of seismic release and could participate in future large ruptures.

References

- Bai, Y., Lay, T., Cheung, K. F., & Ye, L. (2017). Two regions of seafloor deformation generated the tsunami for the 13 November 2016, Kaikōura, New Zealand earthquake. *Geophysical Research Letters*, 44, 6597–6606. https://doi.org/10.1002/2017GL073717
- Bannister, S., & Gledhill, K. (2012). Evolution of the 2010–2012 Canterbury earthquake sequence. New Zealand Journal of Geology and Geophysics, 55(3), 295–304. https://doi.org/10.1080/00288306.2012.680475
- Cesca, S., Zhang, Y., Mouslopoulou, V., Wang, R., Saul, J., Savage, M. K., et al. (2017). Complex rupture process of the M_w 7.8, 2016, Kaikōura earthquake, New Zealand and its aftershock sequence. *Earth and Planetary Science Letters*, 478, 110–120. https://doi.org/10.1016/j.epsl.2017.08.024
- Clark, K., Nissen, E., Howarth, J., Hamling, I., Mountjoy, J., Ries, W., et al. (2017). Highly variable coastal deformation in the 2016 M_w 7.8 Kaikõura earthquake reflects rupture complexity along a transpressional plate boundary. *Earth and Planetary Science Letters*, 474, 334–344. https://doi.org/10.1016/j.epsl.2017.06.048
- Du, W., Thurber, C. H., Reyners, M., Eberhart-Phillips, D., & Zhang, H. (2004). New constraints on seismicity in the Wellington region of New Zealand from relocated earthquake hypocentres. *Geophysical Journal International*, 158, 1088–1102. https://doi.org/10.1111/j.1365-246X.2004.02366.x
- Duputel, Z., & Rivera, L. (2017). Long-period analysis of the 2016 Kaikōura earthquake. *Physics of the Earth and Planetary Interiors*, 265, 62–66. https://doi.org/10.1016/j.pepi.2017.02.004
- Eberhart-Philips, D., & Bannister, S. (2015). 3-D Imaging of the northern Hikurangi subduction zone, New Zealand: Variations in subducted sediment, slab fluids and slow slip. *Geophysical Journal International*, 201(2), 838–855. https://doi.org/10.1093/gji/ggv057
 Eberhart-Phillips, D., Bannister, S., & Ellis, S. (2014). Imaging P and S attenuation in the termination region of the Hikurangi subduction zone, New Zealand. *Geophysical Journal International*, 198(1), 516–536. https://doi.org/10.1093/gji/ggu151

Acknowledgments

This work was supported by the NSF awards EAR-1717119 and EAR-1756075, in conjunction with grants from the New Zealand Earthquake Commission (projects 18/753 and 18/755, the EQC Programme in Seismology and Fault Mechanics at Victoria University of Wellington), and the Marsden Fund of the Royal Society of New Zealand (17-VUW-121). Megan Kortink was supported by a Victoria University of Wellington Summer Scholarship. The STREWN deployment was funded by NSF award EAR-1717119, and instruments were provided by the PASSCAL Instrument Center at New Mexico Tech, University of Auckland, Tulane University, Victoria University of Wellington, and GNS Science. Data collected during the STREWN experiment are available through the IRIS Data Management Center (network code Z1). The facilities of the IRIS Consortium are supported by the NSF under Cooperative Agreement EAR-1261681 and the DOE National Nuclear Security Administration. Waveform and earthquake catalog data from GeoNet are available from http://www.geonet.org. nz. The catalog comprising arrival times, final relocations and related uncertainties is included in the Supporting Information in QuakeML format.



- Eberhart-Phillips, D., Bannister, S., & Reyners, M. (2017). New Zealand Wide model 2.1 seismic velocity model for New Zealand (Version 2.1) [Data set]. Zenodo. http://doi.org/10.5281/zenodo.1043558
- Eberhart-Phillips, D., & Reyners, M. (2012). Imaging the Hikurangi plate interface region with improved local-earthquake tomography. Geophysical Journal International, 190(2), 1221–1242. https://doi.org/10.1111/j.1365-246X.2012.05553.x
- Evans, J. R., Eberhart-Phillips, D., & Thurber, C. H. (1994). User's manual for SIMULPS12 for imaging V_P and V_P/V_S : A derivative of the Thurber tomographic inversion SIMUL3 for local earthquakes and explosions, US Geological Survey Open File Report OFR 94-431, p. 101.
- Evanzia, D., Lamb, S., Savage, M. K., & Stern, T. (2018). Illumination of deformation by bending stresses and slab pull within the Southern Hikurangi Double Benioff Zone. *New Zealand Journal of Geology and Geophysics*, 62(1), 111–120. https://doi.org/10.1080/00288306.2018.1532439
- Gledhill, K., Ristau, J., Reyners, M., Fry, B., & Holden, C. (2011). The Darfield (Canterbury, New Zealand) M_w 7.1 Earthquake of September 2010: A preliminary seismological report. Seismological Research Letters, 82, 378–386. https://doi.org/10.1785/gssrl.82.3.378
- Gusman, A. R., Satake, K., Gunawan, E., Hamling, I., & Power, W. (2018). Contribution from multiple fault ruptures to tsunami generation during the 2016 Kaikōura earthquake. Pure and Applied Geophysics, 175(8), 2557–2574. https://doi.org/10.1007/s00024-018-1949-z
- Hamling, I., Hreinsdóttir, S., Clark, K., Elliott, J., Liang, C., Fielding, E. J., et al. (2017). Complex multi-fault rupture during the 2016 Mw 7.8 Kaikōura earthquake, New Zealand. Science, 356(6334), eaam7194. https://doi.org/10.1126/science.aam7194
- Hamling, I. J., D'Anastasio, E., Wallace, L. M., Ellis, S., Motagh, M., Samsonov, S., et al. (2014). Crustal deformation and stress transfer during a propagating earthquake sequence: The 2013 Cook Strait sequence, central New Zealand. *Journal of Geophysical Research: Solid Earth*, 119, 6080–6092. https://doi.org/10.1002/2014JB011084
- Holden, C., Kaiser, A., Dissen, R. V., & Jury, R. (2013). Sources, ground motion, and structural response characteristics in Wellington of the 2013 Cook Strait earthquakes. *Bulletin of the New Zealand Society for Earthquake Engineering*, 46, 188–195.
- Hollingsworth, J., Ye, L. L., & Avouac, J. P. (2017). Dynamically triggered slip on a splay fault in the Mw 7.8, 2016 Kaikōura (New Zealand) earthquake. Geophysical Research Letters, 44, 3517–3525. https://doi.org/10.1002/2016GL072228
- Jiang, Z., Huang, D., Yuan, L., Hassan, A., Zhang, L., & Yang, Z. (2018). Coseismic and postseismic deformation associated with the 2016 Mw 7.8 Kaikōura earthquake, New Zealand: fault movement investigation and seismic hazard analysis. Earth, Planets and Space, 70(1). https://doi.org/10.1186/s40623-018-0827-3
- Kaiser, A., Balfour, C., Fry, B., Holden, C., Litchfield, N., Gerstenberger, M., et al. (2017). The 2016 Kaikōura, New Zealand, Earthquake: Preliminary Seismological Report. Seismological Research Letters, 88(3), 727–739. https://doi.org/10.1785/0220170018
- Kearse, J., Little, T. A., Van Dissen, R. J., Barnes, P., Langridge, R., Mountjoy, J., et al. (2018). Onshore to offshore ground-surface and seabed rupture of the Jordan–Kekerengu-Needles fault network during the 2016 M_w 7.8 Kaikōura earthquake, New Zealand. Bulletin of the Seismological Society of America, 108(3B), 1573–1595. https://doi.org/10.1785/0120170304
- Kushnir, A. F., Lapshin, V. M., Pinsky, V. I., & Fyen, J. (1990). Statistically optimal event detection using small array data. *Bulletin of the Seismological Society of America*, 80, 1934–1950.
- Lamb, S., Arnold, R., & Moore, J. D. P. (2018). Locking on a megathrust as a cause of distributed faulting and fault-jumping earthquakes. *Nature Geoscience*, 11(11), 871–875. https://doi.org/10.1038/s41561-018-0230-5
- Lamb, S., & Smith, E. (2013). The nature of the plate interface and driving force of interseismic deformation in the New Zealand plate-boundary zone, revealed by the continuous GPS velocity field. *Journal of Geophysical Research: Solid Earth*, 118, 3160–3189. https://doi.org/10.1002/jgrb.50221
- Langridge, R. M., Ries, W. F., Litchfield, N. J., Villamor, P., Van Dissen, R. J., Rattenbury, M. S., et al. (2016). The New Zealand active faults database: NZAFD250. New Zealand Journal of Geology and Geophysics, 59(1), 86–96. https://doi.org/10.1080/00288306.2015.1112818
- Litchfield, N. J., Villamor, P., Van Divssen, R., Nicol, A., Barnes, P., Barrell, D., et al. (2018). Surface fault rupture from the M_w 7.8 2016 Kaikōura, New Zealand, earthquake and insights into factors controlling multi-fault ruptures. Bulletin of the Seismological Society of America, 108(3B), 1496–1520. https://doi.org/10.1785/0120170300
- Lomax, A., Michelini, A., & Curtis, A. (2009). Earthquake location, direct, global-search methods. In R. A. Meyers (Ed.), Encyclopedia of Complexity and System Science, Part 5 (pp. 2449–2473). New York: Springer. https://doi.org/10.1007/978-0-387-30440-3
- Mesimeri, M., Karakostas, V., Papadimitriou, E., Tsaklidis, G., & Jacobs, K. (2018). Relocation of recent seismicity and seismotectonic properties in the Gulf of Corinth (Greece). *Geophysical Journal International*, 212, 1123–1142. https://doi.org/10.1093/gji/ggx450
- Mouslopoulou, V., Saltogianni, V., Nicol, A., Oncken, O., Begg, J., Babeyko, A., et al. (2019). Breaking a subduction-termination from top to bottom: The large 2016 Kaikōura Earthquake, New Zealand. Earth and Planetary Science Letters, 506, 221–230. https://doi.org/10.1016/j.epsl.2018.10.020
- Nicol, A., Khajavi, N., Pettinga, J. R., Fenton, C., Stahl, T., Bannister, S., et al. (2018). Preliminary geometry, displacement, and kinematics of fault ruptures in the epicentral region of the 2016 M_w 7.8 Kaikōura, New Zealand, earthquake. *Bulletin of the Seismological Society of America*, 108(3B), 1521–1539. https://doi.org/10.1785/0120170329
- Petersen, T., Gledhill, K., Chadwick, M., Gale, N. H., & Ristau, J. (2011). The New Zealand National Seismograph Network. Seismological Research Letters, 82, 9–20. https://doi.org/10.1785/gssrl.82.1.9
- Power, W., Clark, K., King, D., Borrero, J., Howarth, J., Lane, E., et al. (2017). Tsunami runup and tide-gauge observations from the 14 November 2016 M 7.8 Kaikōura earthquake, New Zealand. *Pure and Applied Geophysics*, 174(7), 2457–2473. https://doi.org/10.1007/s00024-017-1566-2
- Rawles, C., & Thurber, C. H. (2015). A non-parametric method for automatic determination of *P*-wave and *S*-wave arrival times: application to local micro earthquakes. *Geophysical Journal International*, 202, 1164–1179. https://doi.org/10.1093/gji/ggv218
- Reyners, M., Eberhart-Phillips, D., & Bannister, S. (2011). Tracking repeated subduction of the Hikurangi Plateau beneath New Zealand. Earth and Planetary Science Letters, 311(1-2), 165–171. https://doi.org/10.1016/j.epsl.2011.09.011
- Thurber, C. H., & Eberhart-Phillips, D. (1999). Local earthquake tomography with flexible gridding. Computers & Geosciences, 25(7), 809–818. https://doi.org/10.1016/S0098-3004(99)00007-2
- Thurber, C. H., Lanza, F., & Roecker, S. (2017). Application of hybrid detection and location scheme to volcanic systems, AGU 2017 Abstract.
- Waldhauser, F., & Ellsworth, W. L. (2000). A double-difference earthquake location algorithm: Method and application to the northern Hayward fault, California. *Bulletin of the Seismological Society of America*, 90(6), 1353–1368. https://doi.org/10.1785/0120000006
- Wallace, L. M., Hreinsdóttir, S., Ellis, S., Hamling, I., D'Anastasio, E., & Denys, P. (2018). Triggered slow slip and afterslip on the southern Hikurangi subduction zone following the Kaikōura earthquake. *Geophysical Research Letters*, 45, 4710–4718. https://doi.org/10.1002/2018GL077385
- Walsh, D., Arnold, R., & Townend, J. (2009). A Bayesian approach to determining and parametrizing earthquake focal mechanisms. Geophysical Journal International, 176(1), 235–255. https://doi.org/10.1111/j.1365-246X.2008.03979.x





- Wang, T., Wei, S., Shia, X., Qiu, Q., Lia, L., Peng, D., et al. (2017). The 2016 Kaikōura earthquake: Simultaneous rupture of the subduction interface and overlying faults. *Earth and Planetary Science Letters*, 482, 44–51.
- Wannamaker, P. E., Caldwell, T. G., Jiracek, G. R., Maris, V., Hill, G. J., Ogawa, Y., et al. (2009). The fluid and deformation regime of an advancing subduction system: Marlborough, New Zealand. *Nature*, 460(7256), 733–736. https://doi.org/10.1038/nature08204
- Williams, C. A., Eberhart-Phillips, D., Bannister, S., Barker, D., Henrys, S., Reyners, M., & Sutherland, R. (2013). Revised interface geometry for the Hikurangi subduction zone, New Zealand. *Seismological Research Letters*, 84, 1066–1073. https://doi.org/10.1785/0220130035
- Williams, J. N., Barrell, D., Stirling, M. W., Sauer, K. M., Duke, G. C., & Hao, K. X. (2018). Surface rupture of the Hundalee fault during the 2016 Mw 7.8 Kaikōura earthquake. *Bulletin of the Seismological Society of America*, 108(3B), 1540–1555. https://doi.org/10.1785/0120170291
- Xu, W., Feng, G., Meng, L., Zhang, A., Ampuero, J. P., Burgmann, T., & Fang, L. (2018). Transpressional rupture cascade of the 2016 Mw 7.8 Kaikōura earthquake, New Zealand. *Journal of Geophysical Research: Solid Earth*, 123, 2396–2409. https://doi.org/10.1002/2017JB015168